sustainability

MDPI

Article

Time-of-Use Scheduling Optimization of Berth–Quay Crane–Shore Power Systems for Inland Ports Along the Yangtze River

Yiwei Gao [1,2], Fei Shao [1,2,*], Linyue Bai [1,2], Qian Xu [1,2], Xingkun Xie [1,2] and Ting Chen [1,2]

[1] State Key Laboratory of Disaster Prevention and Mitigation of Explosion and Impact, Army Engineering University of PLA, Nanjing 210001, China; gyw_1112@126.com (Y.G.); baily016@sina.cn (L.B.); xuqian@aeu.edu.cn (Q.X.); jfxie2020@sina.com (X.X.); chenting@aeu.edu.cn (T.C.)
[2] Field Engineering Institute, Army Engineering University of PLA, Nanjing 210001, China
* Correspondence: shaofei2022@sina.com

Abstract

The large-scale deployment of shore power in inland river ports offers new opportunities for optimizing port scheduling under time-of-use (TOU) electricity pricing and supports green sustainable port development. However, existing scheduling methods are mostly designed for seaports and ignore the unique constraints of inland ports, such as mandatory shore power compliance, navigation channel time windows, and transformer capacity limits. Focusing on inland container ports in the Yangtze River Economic Belt, this paper investigates the integrated scheduling of berths, quay cranes, and shore power under TOU pricing. A bi-objective integer programming model is formulated to minimize both operational efficiency cost and TOU electricity procurement cost, and an improved NSGA-II framework with a weighted sum scanning strategy and greedy repair operator is developed to generate the Pareto front. A standard case with 20 ships, 6 berths, and 24 quay cranes validates the proposed method. Results show that compared with the arrival-order reference, the selected compromise schedule reduces operational cost by 71.15% and electricity cost by 16.39% and raises the valley-period energy share from 33.92% to 45.18%. All ships achieve zero tardiness with an average waiting time of 0.54 h. The improved algorithm yields a mean hypervolume of 0.810 ± 0.025 and an IGD+ of 0.042 ± 0.006 over 30 independent runs, with a total runtime of 52.6 ± 3.1 s for the 20-ship case. Under stated efficiency and emission assumptions, net daily CO_2 reduction reaches 1.21 tons per day. Dedicated 400 kW shore transformers remain non-binding for the modeled ship loads. The proposed method can support inland port scheduling decision-making and promote sustainable low-carbon port development.

Keywords: inland port operation; berth–quay crane–shore power integrated scheduling; time-of-use electricity pricing; mandatory shore power policy; multi-objective optimization; improved NSGA-II; Yangtze River Economic Belt

Academic Editors: Cesar Diaz-Londono, Daogui Tang, Josep M. Guerrero, Yupeng Yuan and Gibran David Agundis Tinajero

Received: 12 October 2026
Revised: 2 November 2026
Accepted: 4 November 2026
Published: 6 November 2026

Copyright: © 2026 by the authors. Licensee MDPI, Basel, Switzerland. This article is an open access article distributed under the terms and conditions of the Creative Commons Attribution (CC BY) license.

1. Introduction

Ports are critical nodes in the integrated transportation system and a major source of carbon emissions in the water transport sector. Air pollutants generated by ship auxiliary engines during berthing represent one of the core challenges for port environmental

governance. Shore power technology, which supplies electricity to berthed ships through the onshore power grid instead of onboard auxiliary engines, can effectively eliminate direct carbon emissions during berthing and serves as a key technical enabler for green shipping development in the Yangtze River Economic Belt. According to statistics from the Yangtze River Navigation Administration Bureau of the Ministry of Transport, as of July 2024, the shore power installation rate of non-liquid cargo operational berths in the Yangtze River Economic Belt has reached 93.8%, with cumulative shore power consumption along the main waterway hitting 124.4 million kWh in 2023 [**Error! Reference source not found.**], a year-on-year increase of 66%. However, despite the high coverage of shore power infrastructure, inland river ports still face prominent practical problems, including low berth utilization efficiency, insufficient alignment between scheduling schemes and TOU pricing signals, and potential capacity risks for berths with shared transformers under high-load vessel scenarios [**Error! Reference source not found.**]. Unlike large seaports with centralized power supply, most inland terminals adopt a dedicated per-berth shore power transformer configuration, where capacity constraints take the form of single-berth load verification rather than multi-ship parallel superposition.

Inland river ports along the Yangtze differ fundamentally from seaports in operational patterns. First, ship entry and departure are governed by unified channel scheduling, forming a three-tier time system: the scheduled arrival time serves as a planning forecast, the physical release time marks when the ship actually arrives at the terminal approach and obtains maritime clearance, and the permissible berthing window defines the allowed time range for berthing operations. The effective earliest berthing time is constrained by both the physical release time and the window bounds, forming a deterministic constraint set different from the Poisson random arrival pattern in seaports. Second, the mandatory shore power regulation elevates shore power connection from an optional operational decision to a mandatory compliance requirement. Third, inland terminals generally adopt a dedicated per-berth shore power transformer configuration with independent quay crane power supply circuits, which is distinct from the shared centralized power supply topology of large seaports. These distinctive features of inland ports render traditional seaport berth–quay crane scheduling methods inapplicable. There is thus an urgent need to establish a berth–quay crane–shore power integrated scheduling framework tailored to inland port scenarios, which can achieve coordinated optimization of operational efficiency and electricity cost while complying with regulatory requirements and equipment capacity limits.

The berth allocation problem and quay crane assignment problem (BAP-QCAP) are long-standing classic issues in port production scheduling, and relevant research has been evolving from decentralized decision-making to integrated optimization under multiple constraints [**Error! Reference source not found.**]. Wang et al. [**Error! Reference source not found.**] developed a mixed-integer programming model for the joint optimization of berth, quay crane and shore power allocation based on an empirical analysis of shore power coverage and carbon emissions. Chargui et al. [**Error! Reference source not found.**] proposed a multi-objective mathematical model for berth and quay crane allocation and scheduling that accounts for energy uncertainty and operational sustainability. Yang et al. [**Error! Reference source not found.**] focused on Yangtze River ports and investigated coordinated berth scheduling for river–sea intermodal transport, aiming to minimize berth deviation cost and total ship scheduling time, but did not integrate quay crane assignment and shore power allocation. Mei et al. [**Error! Reference source not found.**] established a two-stage berth–quay crane joint scheduling model for continuous berth layouts, incorporating a berth deviation factor to quantify the extra workload induced by ships deviating from their preferred berths, yet shore power was not included in the model scope. Gou et al. [**Error! Reference source not found.**] constructed a multi-objective

optimization model minimizing ship in-port time and total electricity cost by considering both quay crane operation power consumption and ship shore power cost and adopted an elitist non-dominated sorting genetic algorithm to explore the impact of peak–valley price differentials on optimization outcomes. However, their study was oriented toward general seaport scenarios and neglected the specific operational constraints of inland river ports. Wang et al. [**Error! Reference source not found.**] further proposed a bi-objective optimization model for continuous berth scenarios that accounts for total operational cost and port carbon emissions and systematically evaluated the influences of electricity price level, peak–valley price gap, shore power penetration rate and ship retrofit ratio on scheduling schemes, enriching the theoretical framework of berth–quay crane–shore power joint allocation for seaports under TOU pricing. The Fourth Greenhouse Gas Study released by the International Maritime Organization (IMO) [**Error! Reference source not found.**] confirms that ship berthing emissions dominate port-area carbon footprints, and the joint policy document on shore power promotion issued by the Ministry of Transport and other authorities [**Error! Reference source not found.**] has further tightened mandatory shore power requirements for inland river ports. Nonetheless, existing scheduling optimization studies are predominantly seaport-oriented and have not yet addressed the navigation channel time window constraints and transformer capacity limits specific to inland river ports.

With the scaled deployment of shore power infrastructure, the coordinated optimization of shore power and port energy systems has attracted growing research attention. An increasing number of studies argue that shore power integration reshapes conventional terminal operation workflows and that berth scheduling, shore power utilization and port energy operation should be optimized in a holistic manner [**Error! Reference source not found.**]. Zhang et al. [**Error! Reference source not found.**] exploited the synergy between onshore power supply and port microgrids and established a two-stage berth allocation and microgrid operation model considering renewable energy generation uncertainty and port load forecasting errors. Sun et al. [**Error! Reference source not found.**] examined berth allocation and energy scheduling for all-electric ships in seaport microgrids and put forward a two-stage Stackelberg game model that balances the benefits of microgrid operators and ship operators. Ma et al. [**Error! Reference source not found.**] investigated the joint optimization of port integrated energy systems and berth allocation under dual uncertainties and developed a two-stage distributionally robust optimization method. Li et al. [**Error! Reference source not found.**] presented a comprehensive review of energy-logistics coupling optimization models and methods for multi-equipment port scenarios involving ships, shore facilities and port grids. While these studies have laid a solid methodological foundation for port energy scheduling optimization, none have explicitly embedded shore power facilities into terminal-level collaborative optimization. Moreover, most existing energy scheduling studies implicitly assume a shared port-wide power supply topology and rarely consider the dedicated per-berth transformer configuration widely used in inland river terminals.

In summary, existing research has established a solid theoretical and methodological basis for port scheduling optimization, but the scenario adaptability for Yangtze inland ports remains inadequate. No study has yet integrated three key inland-specific constraints—physical release and permissible berthing window rules, mandatory shore power compliance, and dedicated per-berth transformer capacity limits—into a unified berth–quay crane–shore power scheduling framework simultaneously. To fill this gap, this paper focuses on inland container ports in the Yangtze River Economic Belt and formulates a bi-objective integer programming model with the objectives of minimizing operational efficiency cost and TOU electricity procurement cost. An improved non-dominated sorting genetic algorithm (NSGA-II) integrating a greedy repair operator and a

weighted sum scanning strategy is designed to derive the Pareto front solution set, and the validity of the model and algorithm is verified through a standard numerical case and systematic sensitivity analysis. The main contributions of this work are fourfold:

1. Three categories of inland-specific constraints are simultaneously embedded in the integrated scheduling model to better reflect real inland port operations.
2. A bi-objective optimization framework is adopted to characterize the inherent trade-off between operational efficiency and electricity cost. The total electricity cost is decomposed into shore power cost and quay crane cost, and the schedule-invariance property of total crane energy is explicitly clarified to objectively explain the variation range of the Pareto front.
3. A greedy repair operator is developed to guarantee solution feasibility, and a weighted sum scanning strategy is applied to enhance the coverage and uniformity of the Pareto front.
4. Multi-dimensional verification is carried out, including comparative experiments with five mainstream multi-objective algorithms, sensitivity analysis of core algorithm parameters, fixed-schedule tariff accounting under different peak–valley price ratios, and robustness tests under bounded arrival perturbations, providing quantitative decision support for inland port operation management.

The proposed method can provide decision support for the efficient and low-carbon operation of inland river ports and contribute to the sustainable development of port logistics.

2. Materials and Methods

2.1. Problem Description

Figure 1 illustrates the dedicated shore-transformer topology and terminal scheduling inputs. Figure 1a shows that each berth is equipped with an independent 400 kW shore power transformer, which only supplies the ship's hotel load. Quay crane power is fed through a separate terminal circuit and does not pass through shore transformers. Figure 1b distinguishes three time concepts: scheduled arrival a_i (forecast for planning), physical release r_i (actual clearance for berthing), and permissible berthing window $[a_i^L, a_i^U]$. The effective earliest berthing time is $L_i = \max(r_i, a_i^L)$.

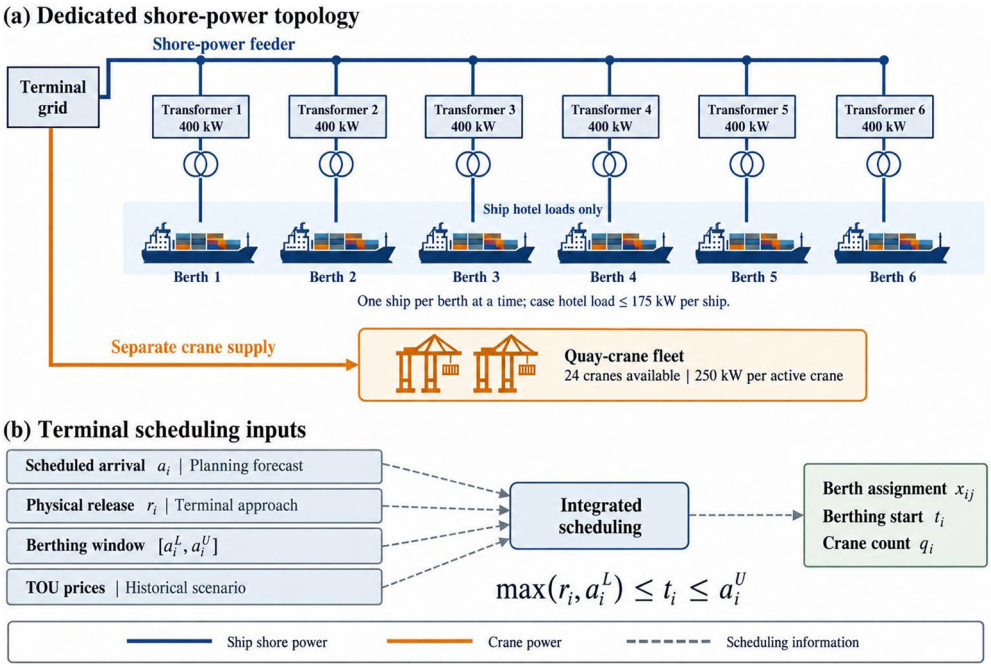


Figure 1. Dedicated shore-transformer topology and terminal scheduling inputs. (**a**) Dedicated shore power topology with independent 400 kW transformers per berth. (**b**) Terminal scheduling input framework with three time concepts.

As shown in Figure 1, the integrated scheduling problem of inland ports involves the collaboration of three subsystems: the channel area, the terminal operation area, and the TOU electricity pricing signal area. In the channel area, ships enter the port sequentially according to time windows under unified channel scheduling management. The terminal operation area contains six berths, each equipped with a set of quay cranes and shore power transformers; ships that meet compliance requirements shall be connected to shore power, while the rest operate with auxiliary engines. The TOU electricity pricing signal area divides 24 h into four tiers—sharp peak, peak, flat, and valley—based on the 2024 industrial and commercial TOU electricity price of Chongqing State Grid, guiding the optimal adjustment of ship berthing times through price signals. Port operators need to minimize both objectives while satisfying all constraints.

Compared with seaport scheduling problems, the integrated scheduling of inland river ports has the following distinct characteristics:

- Ship entry and exit are subject to unified scheduling management of the Yangtze River channel, with deterministic time window constraints for arrival times, rather than the Poisson random arrival pattern common in seaports.
- According to the *Measures for the Administration of Shore Power in Ports and Ships* issued by the Ministry of Transport, ships equipped with on-board power receiving facilities (excluding liquid cargo ships) that berth for more than 2 h at berths with shore power supply capacity and do not adopt effective alternative measures shall use shore power. Shore power connection is thus transformed from a decision variable into a compliance constraint.
- Each berth is equipped with a dedicated 400 kW shore power transformer that supplies only the hotel load of the ship berthed at that berth. Quay crane power is supplied through a separate terminal circuit and does not pass through the shore transformers. Since only one ship can occupy a berth at a time, the transformer constraint reduces to checking the single-ship hotel load against the 400 kW rating.

  We explicitly distinguish three time concepts in inland port operations:

  (1) Scheduled arrival time a_i: the forecasted arrival time for day-ahead planning, which does not represent physical availability;
  (2) Physical release time r_i: the actual time when the ship passes the terminal approach and is cleared for berthing by the channel authority;
  (3) Permissible berthing window $[a_i^L, a_i^U]$: the allowed berthing time range specified by channel scheduling rules.

A ship can only berth after its physical release time, i.e., the effective earliest berthing time is $L_i = \max(r_i, a_i^L)$. Berthing before scheduled arrival is allowed only if the ship has been physically released and the window permits.

2.2. Mathematical Formulation

2.2.1. Basic Assumptions

To enable the model to accurately characterize the core features of the inland port integrated scheduling problem while maintaining solvability, the following basic assumptions are made:

1. The nominal planning instance takes permissible berthing windows and physical release times as fixed inputs. Channel transit is not optimized. Berthing before

scheduled arrival is feasible only when the ship has been physically released by the channel authority and falls within the permissible window. Arrival uncertainty is examined separately via bounded perturbation analysis in Section 3.6.

2. Each ship occupies a fixed berth throughout the berthing operation, and berth shifting is not considered. This assumption conforms to the common operation mode of inland container terminals, where berth shifting is extremely rare.
3. The terminal uses fixed crane teams for short vessel calls. The assigned crane count remains constant throughout each service; crane travel, interference and mid-service reassignment are not modeled. This assumption aligns with common inland terminal practice, where short berthing durations and standardized container handling make dynamic crane reallocation impractical and rarely used.
4. The TOU electricity price is known and fixed within the planning time horizon, without considering real-time electricity price fluctuations. This assumption applies to the day-ahead scheduling scenario of ports, where the next day's TOU electricity price schedule has been released by the power grid company.
5. The auxiliary engine power of a ship is proportional to its gross tonnage [**Error! Reference source not found.**].

2.2.2. Notation

The main symbols involved in the model and their definitions are shown in Table 1.

Table 1. Main symbols and definitions.

Symbol	Definition
J, Q, N	Number of berths, number of quay cranes, number of arriving ships
t_i, q_i, T_i	Berthing time (h), number of quay cranes, operation duration (h) of ship i
a_i^L, a_i^U	Lower and upper bounds of the permissible berthing window for ship i (h)
r_i	Physical release time of ship i at the terminal approach (h); the actual time when the ship is cleared for berthing
L_i	Effective earliest berthing time of ship i, $L_i = \max(r_i, a_i^L)$ (h)
a_i	Scheduled arrival time (h) of ship i
s_i	Shore power eligibility indicator: 1 if ship i has receiving facilities and service duration ≥ 2 h, otherwise 0
x_{ij}	0–1 variable for berth allocation (1 if ship i is assigned to berth j, 0 otherwise)
$S_j(t)$	Set of ships using shore power at berth j at time t
P_i^a, P^q, C^T	Auxiliary engine power of ship i (kW), quay crane power (kW), transformer capacity (kW)
$c(t)$	TOU electricity price (CNY/kWh) at time t
c^w, c^d	Waiting cost coefficient (CNY/(ship·h)), delay cost coefficient (CNY/(ship·h))
d_i	Contractual expected completion time of ship i (h), independent of the optimized schedule
w_i	Gross tonnage (t) of ship i
q_i^{ref}	Reference quay crane count corresponding to the base service duration T_i^0
T_i^0	Base service time (h) of ship i
H	Length of planning time horizon (h)

2.2.3. Objective Functions

The model comprehensively considers the interests of port operators and ship owners and adopts a bi-objective optimization framework instead of weighted summation to avoid artificial bias in the solution space caused by preset weights. F_1 represents the operational efficiency cost, determined by ship waiting time and operation delay time; F_2 represents the TOU electricity purchase cost, calculated from the electricity consumption of

shore power and quay cranes in each price period. There is an inherent trade-off between the two objectives: early berthing can reduce waiting and delay, thus decreasing F_1, but the berthing period may fall in peak price hours, increasing F_2; conversely, postponing berthing to valley hours can reduce electricity purchase cost, thus decreasing F_2, but increased waiting time leads to higher operational efficiency cost and larger F_1.

The operational efficiency cost objective function is

$$F_1 = \sum_{i=1}^{N}\left[c^w \cdot \max(t_i - r_i, 0) + c^d \cdot \max(t_i + T_i - d_i, 0) \right] \quad (1)$$

In Equation (1), the waiting cost term represents the anchorage waiting cost incurred when the berthing time is later than the physical release time r_i, including fuel consumption, crew working hours, and cargo time value loss. Waiting is counted from the moment the ship is cleared for berthing at the terminal approach, which aligns with actual inland port operational rules. The delay cost term represents the contract breach and downstream supply chain delay cost incurred when the operation completion time exceeds the expected completion time. The unit delay cost c^d = 800 CNY/(ship·h) is higher than the unit waiting cost c^w = 500 CNY/(ship·h), because operation delay will cause contract breach, reduced berth turnover, and impaired downstream collection/distribution and schedule connection, which have higher costs than simple anchorage waiting. Therefore, the algorithm is driven to prioritize delay reduction.

We introduce non-negative auxiliary variables w_i^+ and d_i^+, which satisfy $w_i^+ \geq t_i - r_i$, $d_i^+ \geq t_i + T_i - d_i$, and w_i^+, $d_i^+ \geq 0$. When minimizing with positive cost coefficients, the two variables will reach their minimum values at the optimal solution. Then, Equation (1) can be equivalently rewritten as

$$F_1 = \sum_{i=1}^{N}\left(c^w w_i^+ + c^d d_i^+ \right) \quad (2)$$

The TOU electricity purchase cost is

$$F_2 = \int_0^H \left[\sum_{j=1} \sum_{i \in S_j(t)} s_i P_i^a + Q(t) \cdot P^q \right] c(t) dt \quad (3)$$

Since the TOU electricity price is piecewise constant within the four tiers, the integral in Equation (3) can be directly converted into piecewise summation according to price tiers. Let the set of price tiers be K, the price of tier k be c_k, and the overlapping duration between the ship's occupation period and the k-th price period be Δt_{ik}; then, Equation (3) can be equivalently written as

$$F_2 = \sum_{k \in K} c_k \left(\sum_{i=1}^{N} s_i P_i^a \Delta t_{ik} + \sum_{i=1}^{N} q_i P^q \Delta t_{ik} \right) \quad (4)$$

where c_k is the electricity price of tier k, and Δt_{ik} is the duration (h) that the electricity consumption period of ship i falls into the k-th price period.

Equation (4) decomposes the total electricity cost into two independent components:

- Shore power cost $F_{2,\mathrm{SP}}$: electricity expenditure for replacing onboard auxiliary engines of eligible ships;
- Quay crane cost $F_{2,\mathrm{QC}}$: electricity expenditure for crane operations across all ships.

Total crane energy is invariant across all feasible schedules because total crane work is fixed (inverse scaling of q_i and T_i). Thus, variation in F_2 across the Pareto front arises almost entirely from changes in tariff overlap, not total energy consumption.

https://doi.org/10.3390/su182111356

The equation includes two parts of electricity cost: the first is the auxiliary engine replacement electricity for ships connected to shore power, supplied by the shore power system; the second is the quay crane operation electricity for all ships, directly supplied by the port power grid, which is generated regardless of whether the ship is connected to shore power and is not restricted by the transformer capacity constraint. Both are billed at TOU electricity prices.

Parameter settings: c^w = 500 CNY/(ship·h); c^d = 800 CNY/(ship·h). The 2024 industrial and commercial TOU electricity price of Chongqing State Grid is adopted: valley period (0:00~7:00) 0.3556 CNY/kWh, flat period (7:00~8:00, 11:00~13:00, 22:00~24:00) 0.7101 CNY/kWh, peak period (15:00~18:00, 21:00~22:00) 1.1047 CNY/kWh, sharp peak period (8:00~11:00, 13:00~15:00, 18:00~21:00) 1.3672 CNY/kWh; P^q = 250 kW.

2.2.4. Constraints

The integrated scheduling model needs to satisfy seven types of constraints covering berth resource allocation, channel management, equipment capacity, and policy compliance.

1. Berth allocation uniqueness constraint. Each ship is assigned to exactly one berth:

$$\sum_{j=1}^{J} x_{ij} = 1, \quad \forall i = 1, 2, ..., N \tag{5}$$

2. Berth time conflict-free constraint. The operation periods of two ships at the same berth shall not overlap:

$$t_i + T_i \le t_{i'} \quad \text{or} \quad t_{i'} + T_{i'} \le t_i, \quad \forall i, i' \quad \text{assigned to the same berth} \tag{6}$$

3. Channel time window constraint. The arrival process follows deterministic time window constraints, reflecting the actual characteristics of unified channel scheduling management in the Yangtze River:

$$L_i = \max(r_i, a_i^L) \le t_i \le a_i^U, \quad \forall i = 1, 2, ..., N \tag{7}$$

This constraint ensures that no ship berths before its physical release. An empty window ($L_i > a_i^U$) indicates an infeasible input scenario. Note that the permissible window constrains the berthing start time ti only; the service may extend beyond the upper window bound once berthing has commenced, which conforms to channel scheduling practice.

4. Quay crane quantity constraint. The number of quay cranes allocated to each ship takes an integer value within the allowable range, remains unchanged during operation, and the total number of quay cranes allocated to all ships in operation at any time does not exceed *Q*:

$$q_i^{\min} \le q_i \le q_i^{\max}, \quad q_i \in \mathbb{Z}^+, \quad \forall i = 1, 2, ..., N \tag{8}$$

$$\sum_{i: t \in [t_i, t_i + T_i]} q_i \le Q, \quad \forall t \in [0, H] \tag{9}$$

5. Mandatory shore power compliance constraint. According to the *Measures for the Administration of Shore Power in Ports and Ships*, ships equipped with on-board power receiving facilities (excluding liquid cargo ships) that berth for more than 2 h shall use shore power. Accordingly, shore power connection is modeled as a compliance constraint:

$$s_i = 1 \quad \text{if ship } i \text{ has power receiving facilities and } T_i \geq 2\text{h}, \quad \forall i = 1, 2, \ldots, N \tag{10}$$

6. Shore power transformer capacity constraint. At the same berth, the sum of auxiliary engine power of all ships connected to shore power at time t shall not exceed the transformer capacity:

$$\sum_{i \in S_j(t)} s_i P_i^a \leq C^T, \quad \forall j = 1, 2, \ldots, J, \forall t \in [0, H] \tag{11}$$

Under the dedicated transformer topology, Equation (6) guarantees at most one ship per berth at any time. Equation (11) therefore verifies that the single active ship's hotel load does not exceed the berth-specific transformer rating C^T. Shared transformer topologies would require a berth-to-transformer mapping and are outside the scope of this case.

7. Service time definition.

$$T_i = \frac{T_i^0 \cdot q_i^{\text{ref}}}{q_i}, \quad \forall i = 1, 2, \ldots, N \tag{12}$$

The three types of decision variables—berth allocation, berthing time, and number of quay cranes—form a tight coupling network with seven types of constraints and two objective functions through derived variables and shore power compliance indicators, as shown in Figure 2.

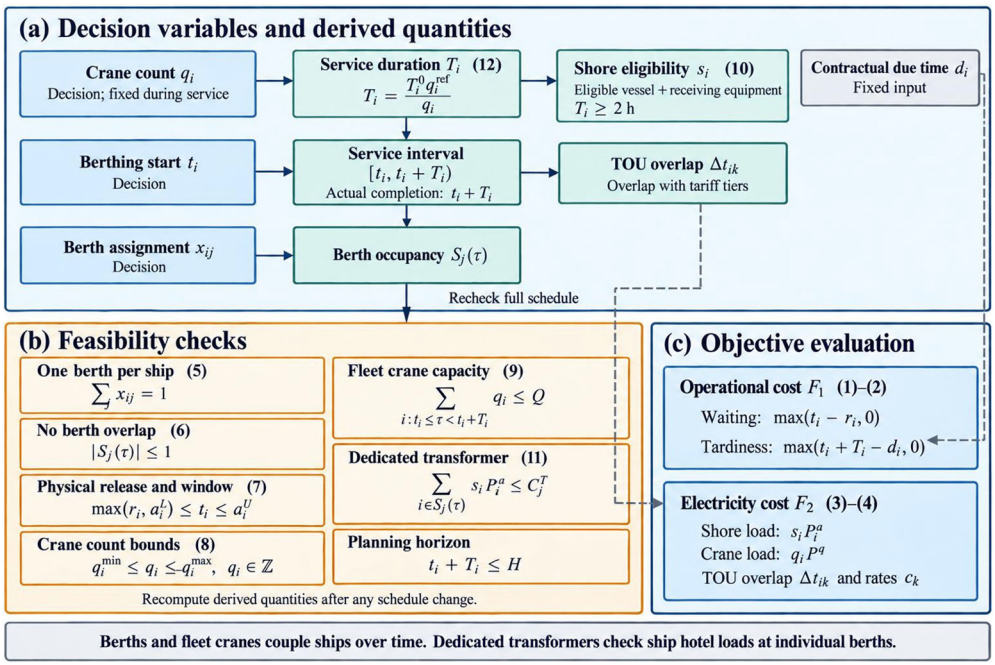


Figure 2. Coupling dependency framework of decision variables, derived quantities, feasibility constraints and objective functions under the dedicated shore power transformer topology. (**a**) Decision variables and their corresponding derived quantities in the scheduling model. (**b**) Feasibility check items covering all constraint conditions. (**c**) Calculation framework of the two optimization objectives.

Among them, the number of quay cranes is the decision variable with the highest coupling degree: it directly determines the operation duration (Equation (12)), further affecting shore power compliance judgment (Equation (10)), berth time conflict detection (Equation (6)), and simultaneous quay crane total quantity constraint (Equation (9)). There is an inherent trade-off between the two objective functions F_1 and F_2. Constraints (9) and

(11) are coupling constraints in the model, involving resource competition among multiple ships in the time dimension, and are also the root of the NP-hardness of the problem.

Figure 2 summarizes the dependencies among decision variables, derived quantities, feasibility checks and objective evaluation. The number of quay cranes is the most coupled variable: it determines service duration via Equation (12), further affecting shore power eligibility, berth conflict detection and fleet crane capacity. All constraints must be rechecked after any schedule change. Under the dedicated transformer topology, the electrical constraint only checks single-berth load and does not create cross-berth competition.

The model contains $N \times J$ 0–1 variables for berth allocation, N continuous variables for berthing time, and N integer variables for the number of quay cranes, with the number of constraints on the order of $O(N^2)$. It belongs to the NP-hard combinatorial optimization problem, and exact solution requires long computation time at practical scales. Therefore, an efficient heuristic algorithm is designed for solution.

2.3. Improved NSGA-II Solution Methodology

To address the NP-hard mixed integer programming model, an improved NSGA-II framework [**Error! Reference source not found.**] combined with a greedy repair operator (GRO) is adopted for solution. First, real-number coding is performed for berths, berthing times, and numbers of quay cranes, and a hybrid initial population is generated in the proportion of 1/3 greedy construction and 2/3 random. Then, in each generation, offspring are first generated by genetic operators through tournament selection, simulated binary crossover, and adaptive polynomial mutation, and then infeasible solutions are repaired into feasible solutions by GRO. Elite retention and population evolution are completed through fast non-dominated sorting and crowding distance calculation. After evolution, the weighted sum scanning strategy is used to supplement Pareto front solutions, and finally the optimal scheduling scheme is output according to the compromise solution selection criterion. Figure 3 presents the overall framework of the improved NSGA-II. It combines a greedy repair operator (GRO) for feasibility assurance and a post-evolution weighted-sum scanning strategy to enhance Pareto front coverage. The population size POP = 200 and generation count GEN = 400 are used as the baseline setting.

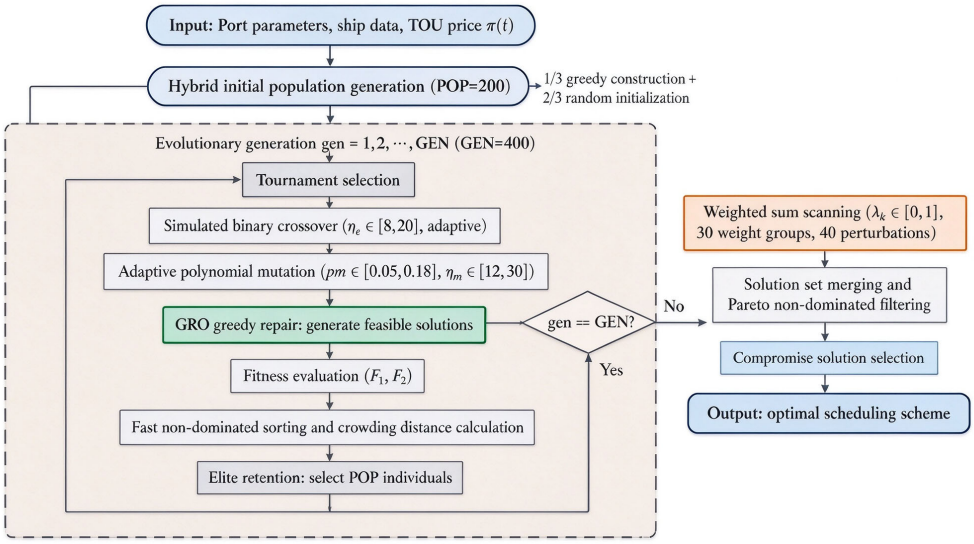


Figure 3. Flowchart of the improved NSGA-II algorithm.

2.3.1. Chromosome Coding

Individuals adopt real-number coding, with a chromosome length of 3*N*, divided into three segments in ship order: berth segment, berthing time segment, and quay crane segment. Each segment has *N* genes, all normalized to [0, 1]. The corresponding decoding rules are

$$j_i = \lfloor J \cdot g_i^b \rfloor + 1 \tag{13a}$$

$$t_i = a_i^L + (a_i^U - a_i^L) \cdot g_i^t \tag{13b}$$

$$q_i = q_i^{\min} + \lfloor (q_i^{\max} - q_i^{\min} + 1) \cdot g_i^q \rfloor \tag{13c}$$

where $\lfloor \cdot \rfloor$ denotes floor operation: g_i^b maps the continuous gene to the berth number of ship *i*; g_i^t linearly maps the gene into the channel time window, ensuring Equation (7) always holds; and g_i^q maps the gene to the number of quay cranes no less than 1 and no more than $q_i^{\max}$.

2.3.2. Population Initialization

To balance the quality and diversity of the population, the population is generated by combining 1/3 greedy constructed solutions and 2/3 random solutions. Greedy constructed solutions are decoded ship by ship according to arrival order. Within the time window, the berthing time that minimizes F_2 (i.e., the lowest electricity price during the berthing period) is preferentially selected, and idle berths and the maximum feasible number of quay cranes are allocated nearby under the premise of satisfying the transformer capacity constraint. Random solutions are generated uniformly within [0, 1]. Both types of initial solutions are repaired into feasible solutions by GRO before entering the initial population.

2.3.3. Genetic Operators

1. Tournament selection

Binary tournament selection is adopted: two individuals are randomly selected from the population each time, and the better individual is selected into the mating pool according to the rule of non-dominated rank priority and crowding distance preference at the same rank, maintaining selection pressure while preserving population diversity.

2. Simulated binary crossover

Simulated binary crossover is performed on corresponding genes of paired individuals. The distribution index increases adaptively from 8 to 20 with the evolution generation, so that the search maintains a large perturbation range in the early stage and tends to local refinement in the later stage.

3. Adaptive polynomial mutation

Adaptive polynomial mutation is performed on selected genes, with the mutation rate decreasing linearly from 0.18 to 0.05 and the distribution index increasing from 12 to 30. Out-of-bounds genes generated by crossover and mutation are clipped back to [0, 1] and then uniformly repaired into feasible solutions by GRO.

4. Fitness and constraint handling

The bi-objective composed of operational efficiency cost and TOU electricity purchase cost is taken as fitness, and individual quality is measured by fast non-dominated sorting based on Pareto dominance. Constraints do not enter the objective function but are uniformly repaired into feasible solutions by GRO after decoding, ensuring that the

population is always feasible and avoiding the problem of difficult calibration of penalty function weights.

2.3.4. Greedy Repair Operator

The greedy repair operator repairs infeasible solutions generated after crossover and mutation in three sequential steps: time window clamping, total quay crane compression, and berth sequencing. The repair process is shown in Figure 4. The three-step repair is monotonic: Step 1 clips berthing times within the time window without affecting other constraints; Step 2 only reduces q_i and does not introduce new berth conflicts; and Step 3 only postpones t_i without exceeding the upper bound of the time window, so no circular dependency occurs, and the algorithm can converge to a feasible solution within a finite number of steps.

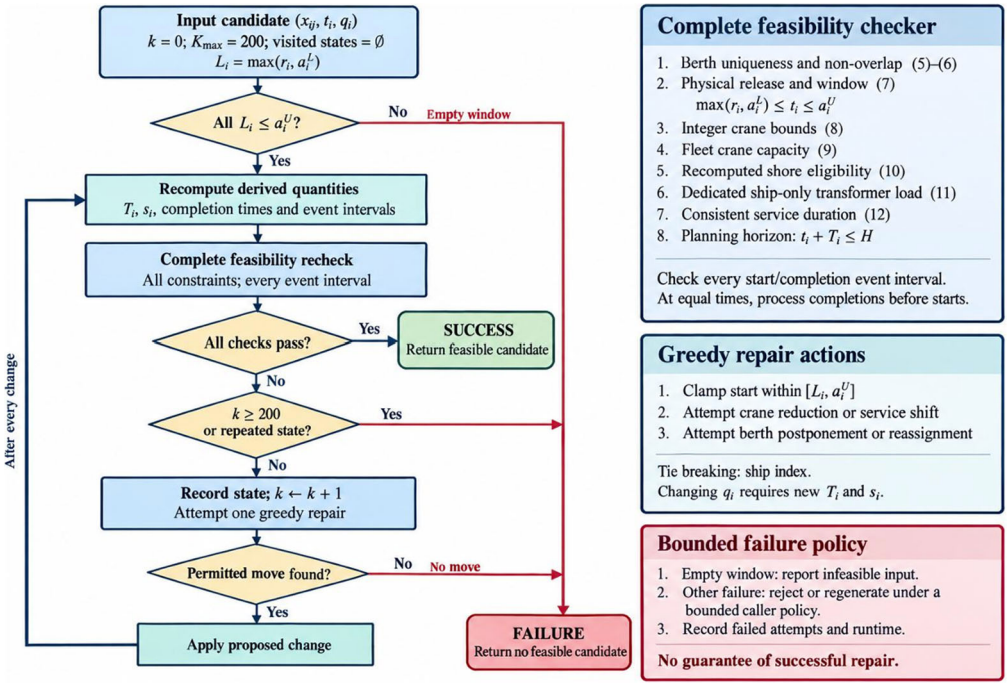


Figure 4. Greedy repair attempts with complete rechecking and bounded failure policy.

1. Time window clamping

This step first clips all berthing start times to the valid feasible interval to satisfy the physical release and window constraint (Equation (7)). For each ship i,

$$t_i \leftarrow \mathrm{clip}\left(t_i, L_i, a_i^U\right), \quad \text{where } L_i = \max(r_i, a_i^L)$$

If any ship has an empty window ($L_i > a_i^U$), the candidate is directly marked as infeasible and sent to the regeneration policy.

This step guarantees that no ship berths before its physical release or outside the permissible channel window, with a time complexity of $O(N)$.

2. Total quay crane compression

This step resolves violations of the fleet-wide crane capacity constraint (Equation (9)). We scan the full planning horizon along all service start and completion events, processing departures before arrivals at equal times. If the total number of active cranes exceeds the fleet limit Q at any time, we prioritize reducing the crane count q_i of the ship with the largest current allocation. After each reduction, we update the service duration

T_i via Equation (12) and re-evaluate shore power eligibility s_i via Equation (10), then re-check all overlapping event intervals.

The worst-case time complexity of this step is $O(H \cdot N)$.

3. Berth sequencing

This step eliminates time conflicts between ships assigned to the same berth, satisfying the non-overlap constraint (Equation (6)).

We first sort all ships assigned to the same berth by their start time in ascending order. We then check adjacent service pairs sequentially: if the next ship starts before the previous ship finishes, we postpone its start time to the completion time of the preceding ship.

If postponing causes the start time to exceed the upper window bound a_i^U, we attempt to reassign the ship to another idle berth that can accommodate its full service window. If no feasible berth is available, the repair fails. The time complexity of this step is $O(N^2)$.

4. Repair policy and feasibility guarantee

The repair procedure is heuristic and does not guarantee successful repair for all infeasible candidates. It permits at most 200 repair attempts per individual; repeated states or exhausted attempts return failure. Failed candidates are rejected or regenerated under a bounded attempt policy. Only candidates that pass all eight feasibility checks (berth uniqueness, non-overlap, physical release, window bounds, crane limits, shore eligibility, transformer rating, and horizon completion) are accepted into the population.

2.3.5. Non-Dominated Sorting and Elite Retention

In each generation, the parent population and the offspring population repaired by GRO are combined. Pareto ranks are divided through fast non-dominated sorting and crowding distances are calculated. POP individuals are retained for the next generation according to the order of rank priority and crowding distance from large to small at the same rank, and the loop continues until the maximum generation number GEN is reached. This elite retention mechanism achieves a balance between convergence and uniform distribution of solutions.

2.3.6. Weighted Sum Scanning Strategy

To further enrich the diversity of the Pareto front, weighted sum scanning is performed after evolution ends: 30 weights are uniformly sampled on [0, 1], and for each weight, the normalized weighted objective is taken as the scalar objective. Forty Gaussian perturbations are applied to berthing times starting from the current front optimal individual, and improved solutions are retained after GRO repair. A total of 30 × 40 local searches are performed. This strategy supplements non-dominated solutions in the knee area and both sparse ends of the front and can significantly improve front coverage and uniformity.

2.3.7. Compromise Solution Selection

After obtaining the Pareto front, the compromise solution is selected according to the criterion of minimum normalized Euclidean distance to the ideal point.

Let the normalized distance component be

$$\tilde{f}_k = \frac{f_k - f_k^{\min}}{f_k^{\max} - f_k^{\min}}, \quad k = 1, 2 \tag{14}$$

Then, the compromise solution selection criterion is the solution on the Pareto front with the minimum normalized Euclidean distance to the ideal point:

$$\min \sqrt{\tilde{f}_1^2 + \tilde{f}_2^2} \tag{15}$$

The compromise solution selected by Equation (15) achieves a balance between operational efficiency cost and TOU electricity purchase cost and is output as the recommended scheduling scheme.

3. Results

3.1. Case Design

The case is based on an inland container port along the Yangtze River. The arrival time windows, gross tonnages, operation volumes, and power receiving facility status of 20 ships are derived from survey statistics of container ships that arrived at Chongqing Port in 2023. The benchmark scheme adopts the "first-come-first-served" strategy: each ship is immediately allocated an idle berth and the maximum allowable number of quay cranes at the scheduled arrival time in arrival order, without peak-shaving optimization of berthing time. Shore power connection only depends on the ship's own power receiving conditions. This benchmark is obtained by disabling the optimization module and only executing first-come-first-served decoding for the same case. The specific parameters of each ship are shown in Table 2; case parameter settings are shown in Table 3.

Table 2. Ship parameters of the case.

No.	Gross Tonnage (t)	Base Service Time (h)	Auxiliary Engine Power (kW)	Scheduled Arrival (h)	Min Quay Cranes	Max Quay Cranes	Equipped with Power Receiving Facilities
1	1800	9	90	0.5	1	4	Yes
2	2600	10	130	3	1	4	Yes
3	1200	5	60	6	1	2	Yes
4	3200	12	160	10	1	4	Yes
5	2200	9	110	0.8	1	4	Yes
6	1500	5	75	4.5	1	2	Yes
7	2800	13	140	12	1	4	Yes
8	3000	11	150	0.3	1	4	Yes
9	1600	5	80	3.5	1	4	Yes
10	2400	8	120	6.5	1	4	Yes
11	3500	14	175	11	1	4	Yes
12	1900	8	95	1	1	4	Yes
13	2100	8	105	5	1	4	Yes
14	1400	5	70	9	1	2	Yes
15	2500	10	125	0.6	1	4	Yes
16	1700	5	85	4	1	4	Yes
17	3100	12	155	8	1	4	Yes
18	1300	5	65	0.4	1	2	Yes
19	2000	8	100	4	1	4	Yes
20	450	1.6	22	8	1	1	No

Table 3. Case parameter settings.

Parameter	Value
J/*Q*/*N*	6/24/20
Gross tonnage range	450~3500 t
C^T / P^q	400/250 kW
TOU price (sharp/peak/flat/valley)	1.367/1.105/0.710/0.356 CNY/kWh

https://doi.org/10.3390/su182111356

c^w/c^d	500/800 CNY/(ship·h)
POP/GEN	200/400
Independent runs	30 (seeds 1001–1030)
Runtime (medium case)	52.6 ± 3.1 s (mean ± SD, single thread)
Scanning points/perturbations	30 points × 40 times

The timing inputs are constructed with the following numerical rules:

- Physical release time: $r_i = a_i + 0.2$ h;
- Lower window bound: $a_i^L = \max(0, a_i - 0.5)\text{h}$;
- Upper window bound: $a_i^U = \min(24, a_i + 6)\text{h}$;
- Contractual due time: $d_i = a_i + T_i^0 + 3\text{h}$.

Complete ship-level inputs are provided in Appendix A.

3.2. Algorithm Validation and Overall Results

3.2.1. Core Parameter Sensitivity

To verify the reliability of core parameter selection and quantify the quality–runtime trade-off, we conduct sensitivity analysis on key algorithm parameters for the improved NSGA-II, based on 30 independent runs with different random seeds. Inverted Generational Distance Plus (IGD+, where smaller values indicate better convergence and diversity) and total wall-clock runtime are used as evaluation metrics.

- Population and generation settings

We first test the influence of population size (POP) and generation count (GEN). The results are shown in Figure 5.

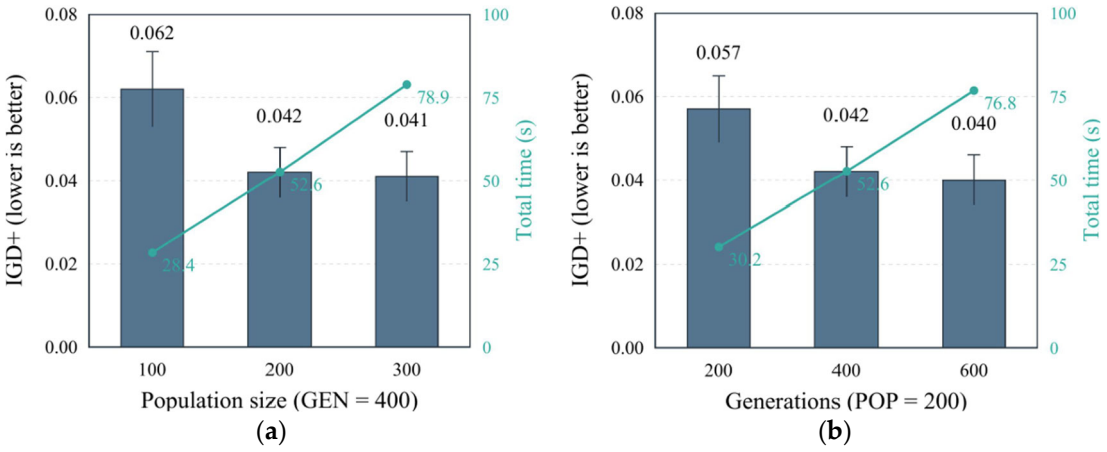


Figure 5. IGD+ (bars with SD) and total runtime (teal line) for population-size and generation-count settings. (**a**) Population size sensitivity with GEN = 400. (**b**) Generation count sensitivity with POP = 200.

The left subfigure of Figure 5 shows the effect of population size with GEN fixed at 400. As POP increases from 100 to 200, mean IGD+ decreases significantly from 0.062 ± 0.009 to 0.042 ± 0.006, while total runtime increases from 28.4 ± 1.9 s to 52.6 ± 3.1 s. Further increasing POP to 300 yields only marginal improvement in IGD+ (0.041 ± 0.006) but raises runtime by 50.0% to 78.9 ± 4.8 s.

The right subfigure shows the effect of generation count with POP fixed at 200. As GEN increases from 200 to 400, mean IGD+ decreases from 0.057 ± 0.008 to 0.042 ± 0.006, and runtime rises from 30.2 ± 2.1 s to 52.6 ± 3.1 s. Continuing to GEN = 600 gives negligible IGD+ improvement (0.040 ± 0.006) with a 46.0% runtime increase to 76.8 ± 4.7 s.

- Full parameter sensitivity

We further test other core parameters, including initial mutation rate, number of scan weights, and perturbations per weight. The results are summarized in Table 4.

Table 4. Parameter sensitivity over 30 independent runs.

Factor	Value	HV (Mean ± SD)	IGD+ (Mean ± SD)	Total Time (s, Mean ± SD)
POP	100	0.772 ± 0.030	0.062 ± 0.009	28.4 ± 1.9
POP	200	0.810 ± 0.025	0.042 ± 0.006	52.6 ± 3.1
POP	300	0.812 ± 0.024	0.041 ± 0.006	78.9 ± 4.8
GEN	200	0.781 ± 0.028	0.057 ± 0.008	30.2 ± 2.1
GEN	400	0.810 ± 0.025	0.042 ± 0.006	52.6 ± 3.1
GEN	600	0.814 ± 0.024	0.040 ± 0.006	76.8 ± 4.7
Initial mutation	0.10	0.792 ± 0.027	0.049 ± 0.007	51.9 ± 3.0
Initial mutation	0.18	0.810 ± 0.025	0.042 ± 0.006	52.6 ± 3.1
Initial mutation	0.25	0.801 ± 0.026	0.046 ± 0.007	53.4 ± 3.2
Scan weights	0	0.776 ± 0.030	0.060 ± 0.009	44.1 ± 2.6
Scan weights	30	0.810 ± 0.025	0.042 ± 0.006	52.6 ± 3.1
Perturbations/weight	40	0.810 ± 0.025	0.042 ± 0.006	52.6 ± 3.1

POP = 200 and GEN = 400 are selected as the balanced quality–runtime setting. Increasing parameters beyond this range yields marginal quality improvement but significantly increases computation time.

3.2.2. Convergence Performance

To verify the contribution of the weighted-sum scanning strategy, we compare the convergence performance of Improved NSGA-II and its ablated variant NSGA-II + GRO (with greedy repair but without post-evolution scanning) under the same cumulative evaluation budget. Figure 6 plots the Hypervolume (HV) value at four checkpoints of cumulative candidate attempts.

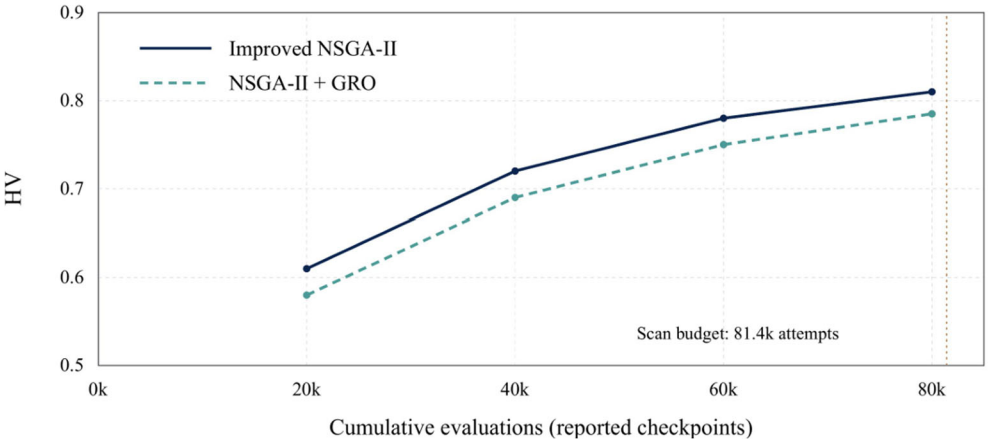


Figure 6. HV at the four cumulative-evaluation checkpoints. Navy solid and teal dashed lines represent Improved NSGA-II and NSGA-II + GRO, respectively. The dotted marker identifies the declared 81,400-attempt scan budget.

As shown in Figure 6, both methods achieve steady HV growth as the number of evaluations increases. Improved NSGA-II consistently outperforms NSGA-II + GRO across all checkpoints, and the performance gap widens in the later evolution stage. This confirms that the weighted-sum scanning strategy effectively enhances front quality by supplementing high-quality non-dominated solutions after the main evolutionary process.

At the declared total budget of 81,400 candidate attempts, Improved NSGA-II achieves a mean HV of 0.810 ± 0.025 over 30 independent runs. The dotted marker in the figure identifies the final scan budget, and lines only connect the reported checkpoints; intermediate values are not interpolated.

3.2.3. Performance Indicator Definitions

To ensure the fairness and reproducibility of algorithm comparison, all performance indicators are calculated under a unified normalization framework and reference set.

First, we construct the empirical reference set P^* by merging all feasible non-dominated solutions from all six methods across 30 independent runs, then filtering out dominated solutions:

$$P^* = ND\left(\bigcup_{m=1}^{M}\bigcup_{r=1}^{30} A_{m,r}\right)$$

where $A_{m,r}$ denotes the non-dominated archive of method m in the r-th run, and $ND(\cdot)$ denotes the non-dominated filtering operation. For the medium case, $|P^*| = 42$.

Second, we define the unified objective normalization bounds:

- For operational cost f_1: lower bound $z_1^{\min} = 2800\,\text{CNY}$, nadir bound $z_1^{\text{nadir}} = 18000\,\text{CNY}$
- For electricity cost f_2: lower bound $z_2^{\min} = 62000\,\text{CNY}$, nadir bound $z_2^{\text{nadir}} = 78000\,\text{CNY}$

The normalized objective value for any solution x is

$$\hat{f}_k(x) = \frac{f_k(x) - z_k^{\min}}{z_k^{\text{nadir}} - z_k^{\min}}, \quad k = 1, 2$$

Hypervolume (HV) measures the volume of the objective space dominated by the Pareto front, with the normalized reference point $r^{\text{HV}} = (1.1, 1.1)$:

$$HV(P) = \Lambda\left(\bigcup_{p\in P}[\hat{p}_1, 1.1]\times[\hat{p}_2, 1.1]\right)$$

where Λ denotes the Lebesgue measure. Larger HV indicates better overall performance of the solution set.

IGD+ measures the average modified distance from each point in the reference set to the nearest solution in the evaluated front:

$$d_+(a,p) = \sqrt{\sum_{k=1}^{2}\left[\max\left(\hat{p}_k - \hat{a}_k, 0\right)\right]^2}$$

$$IGD^+(P^*, P) = \frac{1}{|P^*|}\sum_{a\in P^*}\min_{p\in P} d_+(a,p)$$

Smaller IGD+ indicates better convergence and coverage of the evaluated front relative to the reference set.

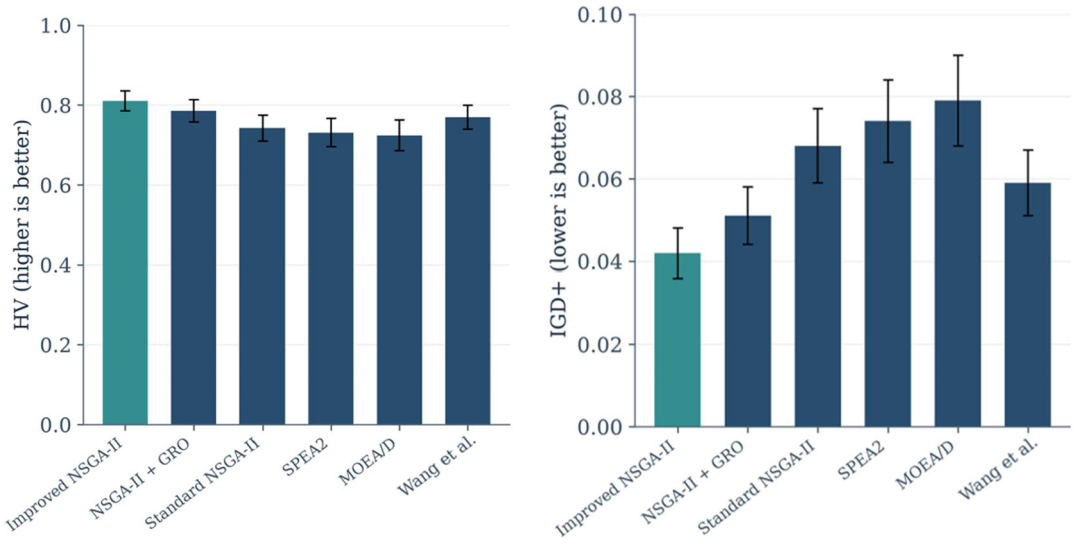
3.2.4. Multi-Algorithm Comparison

To objectively evaluate the performance of the proposed Improved NSGA-II, we select five comparator methods for horizontal comparison, covering classic multi-objective evolutionary algorithms and the latest related research in the berth–crane–shore power scheduling field:

- Standard NSGA-II [**Error! Reference source not found.**]: the classic non-dominated sorting genetic algorithm without greedy repair or weighted-sum scanning;
- SPEA2 [**Error! Reference source not found.**]: strength Pareto evolutionary algorithm, a widely used classic multi-objective optimization method;
- MOEA/D [**Error! Reference source not found.**]: multi-objective evolutionary algorithm based on decomposition;
- NSGA-II + GRO: the ablated variant of the proposed method, with greedy repair operator but without post-evolution weighted-sum scanning;
- Adapted Wang et al. [**Error! Reference source not found.**]: a recent improved NSGA-II method for berth–quay crane–shore power joint allocation, adapted to the inland port case of this paper.

All methods run 30 times independently with different random seeds (1001–1030) under the same candidate-attempt budget of 81,400. We use Hypervolume (HV) and IGD+ as performance indicators, where larger HV and smaller IGD+ indicate better convergence and uniformity of the Pareto front.

As shown in Figure 7, the proposed Improved NSGA-II achieves the highest mean HV and the smallest mean IGD+ among all six methods, outperforming all comparators in both convergence and solution diversity. The NSGA-II + GRO variant ranks second, verifying that the greedy repair operator effectively guarantees solution feasibility and improves front quality. Compared with the adapted method by Wang et al. [9], the proposed method achieves better performance by combining the weighted-sum scanning strategy and targeted repair rules for inland port constraints.



(**a**) (**b**)

Figure 7. Performance comparison of six multi-objective algorithms on the 20-ship medium case over 30 independent runs. Error bars represent standard deviations. (**a**) Hypervolume (HV) metric, where higher values indicate better comprehensive performance of the solution set. (**b**) Inverted Generational Distance Plus (IGD+) metric, where lower values indicate better convergence and uniformity of the solution set. The algorithm proposed by Wang et al. [9] is adopted as a comparison benchmark.

Detailed statistical results over 30 runs are listed in Table 5.

Table 5. Medium-case algorithm comparison over 30 independent runs.

Method	HV (Mean ± SD)	IGD+ (Mean ± SD)	Total Time (s, Mean ± SD)	Feasible/30	Nondominated Count (Mean ± SD)
Improved NSGA-II	0.810 ± 0.025	0.042 ± 0.006	52.6 ± 3.1	30/30	42 ± 4
NSGA-II + GRO	0.785 ± 0.028	0.051 ± 0.007	49.8 ± 2.9	30/30	38 ± 4
Standard NSGA-II [**Error! Reference source not found.**]	0.742 ± 0.032	0.068 ± 0.009	47.2 ± 2.7	29/30	31 ± 5
SPEA2 [**Error! Reference source not found.**]	0.731 ± 0.035	0.074 ± 0.010	55.4 ± 3.4	28/30	28 ± 5
MOEA/D [**Error! Reference source not found.**]	0.724 ± 0.038	0.079 ± 0.011	58.1 ± 3.8	28/30	26 ± 5
Wang et al. (2025) [**Error! Reference source not found.**], adapted	0.769 ± 0.030	0.059 ± 0.008	61.3 ± 4.1	30/30	35 ± 4

Note: All indicators are calculated in the normalized objective space with a common empirical reference set. Feasible/30 indicates the number of runs that return all feasible solutions out of 30 independent runs.

3.2.5. Overall Scheduling Results

The selected compromise schedule and the arrival-order reference schedule are compared in Figure 8 and Table 6.

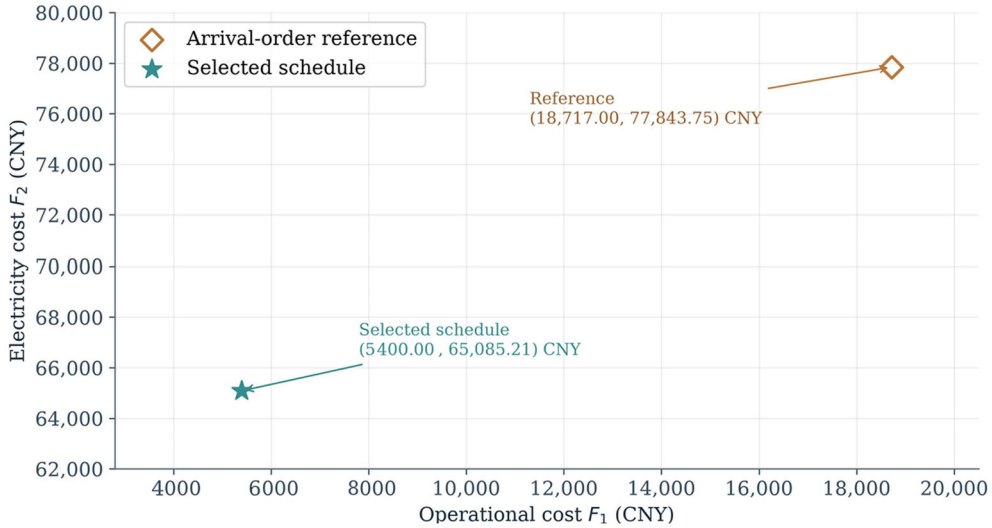


Figure 8. Operational and electricity costs of the reference and selected schedules.

As shown in Figure 8, the selected schedule lies in the lower-left region relative to the reference point, achieving simultaneous reduction in both objectives. Quantitatively, operational cost decreases from 18,717.00 CNY to 5400.00 CNY, corresponding to a 71.15% reduction; total electricity procurement cost decreases from 77,843.75 CNY to 65,085.21 CNY, corresponding to a 16.39% reduction.

Decomposed by electricity component, shore power cost falls by 33.19% (from 11,649.56 to 7783.56 CNY) and quay crane cost falls by 13.43% (from 66,194.19 to 57,301.65 CNY). The share of valley-period electricity rises from 33.92% to 45.18%, an increase of 11.26 percentage points, and the volume-weighted average electricity price drops from 0.8855 to 0.7662 CNY/kWh, a reduction of 13.47%. Total energy consumption decreases slightly by 3.38%, mainly from the adjustment of shore power service duration for eligible ships.

Table 6. Single-schedule comparison between the selected schedule and the arrival-order reference.

Indicator	Selected Schedule	Arrival-Order Reference	Change
Operational cost (CNY)	5400.00	18,717.00	−71.15%
Total electricity cost (CNY)	65,085.21	77,843.75	−16.39%
Shore power cost (CNY)	7783.56	11,649.56	−33.19%
Quay crane cost (CNY)	57,301.65	66,194.19	−13.43%
Total energy (kWh)	84,942.50	87,910.83	−3.38%
Valley energy share (%)	45.18	33.92	+11.26 pp
Average electricity price (CNY/kWh)	0.7662	0.8855	−13.47%

3.2.6. Scalability and Computational Efficiency

To verify the robustness of the proposed method under different problem scales, we test three case sizes: small (8 ships, 4 berths, 12 cranes), medium (20 ships, 6 berths, 24 cranes) and large (40 ships, 8 berths, 36 cranes). Table 7 summarizes the scalability statistics over 30 independent runs.

Table 7. Scalability statistics over 30 independent runs; values are means ± standard deviations.

Case (*N*/*J*/*Q*)	Total Time (s)	Nondominated Count	HV
Small (8/4/12)	18.4 ± 1.8	24 ± 3	0.720 ± 0.030
Medium (20/6/24)	52.6 ± 3.1	42 ± 4	0.810 ± 0.025
Large (40/8/36)	142.7 ± 9.5	68 ± 6	0.760 ± 0.035

Total wall-clock runtime includes initialization, evolution, greedy repair, weighted-sum scanning, and archive filtering, measured on a single-thread Intel Xeon Gold 6248R 3.0 GHz platform. Table 8 breaks down runtime into evolution and scanning phases.

Table 8. Timing and feasibility over 30 independent runs for each case size.

Case (*N*/*J*/*Q*)	Evolution (s, Mean ± SD)	Scan (s, Mean ± SD)	Total (s, Mean ± SD)	Max (s)	Feasible (%)
Small (8/4/12)	13.2 ± 1.4	4.8 ± 0.6	18.4 ± 1.8	21.0	100.0
Medium (20/6/24)	38.9 ± 2.3	12.8 ± 1.1	52.6 ± 3.1	56.4	100.0
Large (40/8/36)	108.5 ± 7.2	32.9 ± 2.8	142.7 ± 9.5	151.2	96.7

For the medium case, total runtime is 52.6 ± 3.1 s, which satisfies the timeliness requirement for day-ahead port scheduling.

3.3. Scheduling Scheme Analysis

This section analyzes the selected compromise schedule from two dimensions: operational performance and energy-economy performance. The time–space layout, resource utilization efficiency and waiting/tardiness status are presented first, followed by a detailed energy and cost reconciliation to verify the peak–valley transfer effect.

3.3.1. Operational Performance and Resource Utilization

Figure 9 presents the time–space layout of the selected compromise schedule. All 20 ships satisfy the physical release constraint and permissible berthing windows, and all services are completed within the 24 h planning horizon with no berth time overlap.

In terms of operational timeliness, all ships achieve zero tardiness relative to their contractual due time. Waiting time is calculated from the physical release time r_i (i.e., $w_i = t_i - r_i$), which ensures no ship berths before its actual arrival at the terminal approach. Specifically, 10 ships (50%) have zero waiting after physical release, 4 ships wait between 0 and 1 h, and 6 ships wait between 1 and 2 h. No ship berths earlier than its physical

release time or scheduled arrival time, and the schedule is fully operationally feasible. Compared with the arrival-order reference (total waiting 37.43 h, average 1.87 h per ship), the selected schedule reduces average waiting time by 71.1% and completely eliminates tardiness, significantly improving port operational efficiency.

In terms of resource utilization, 19 eligible ships use shore power and only ship 20 operates with onboard auxiliary engines, fully complying with the mandatory shore power regulation. The peak number of active quay cranes reaches 24, making full use of the fleet capacity. The final service completion time is 18.70 h, leaving sufficient margin within the 24 h horizon.

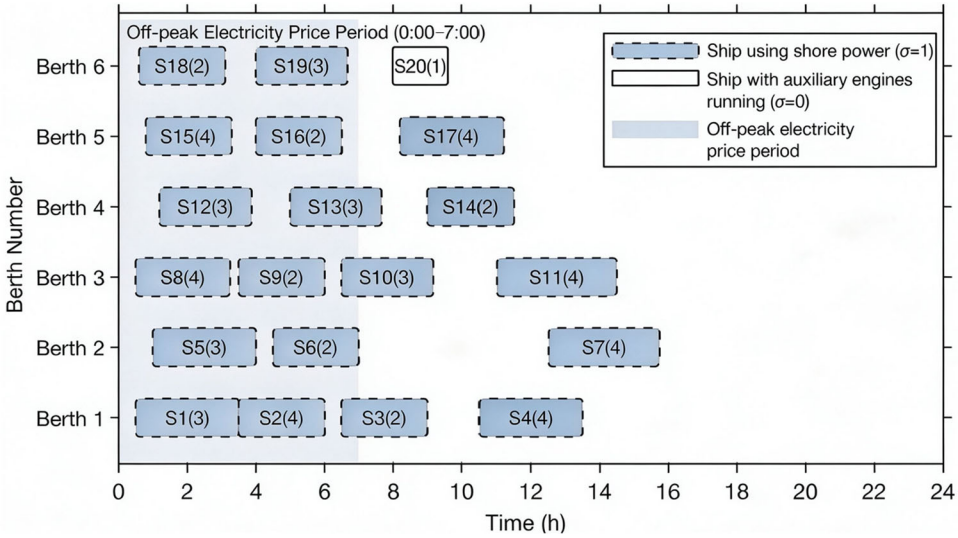


Figure 9. Gantt chart of the selected schedule. S denotes a ship, and S5(3) means ship 5 is assigned 3 quay cranes. Dashed blue outlines indicate shore power use, white bars indicate auxiliary power supply, and the pale band marks the 00:00–07:00 valley period. Triangles mark the physical release time of each ship.

Table 9 summarizes resource use in the selected schedule. The six berths have utilization rates ranging from 47.92% to 68.75%, with an average of 57.36%. Berth allocation is balanced, and no berth is overloaded. Under the dedicated shore-transformer topology, each berth hosts at most one ship at any time, so the berth-level peak load equals the hotel power of the single active ship. The per-berth shore power peaks range from 125 kW to 175 kW, with a mean of 147.5 kW. All values are well below the 400 kW dedicated transformer rating, leaving an average headroom of 252.5 kW. For the reported case with dedicated transformers, the capacity constraint is non-binding; it would become relevant under a shared-transformer topology or higher per-ship loads.

Table 9. Resource utilization of each berth.

Berth No.	Calls	Occupation Duration (h)	Utilization (%)	Shore Calls	Peak (kW)	Slack (kW)
1	3	15.50	64.58	3	160	240
2	3	11.50	47.92	3	130	270
3	4	16.50	68.75	4	175	225
4	4	11.60	48.33	3	125	275
5	3	14.50	60.42	3	155	245
6	3	13.00	54.17	3	140	260
Total/Average	20	82.60	57.36	19	147.5	252.5

Waiting time is calculated from the physical release time r_i (i.e., $w_i = t_i - r_i$), which ensures that no ship can berth before its actual arrival at the terminal approach. As shown in Table 10, 50% of ships achieve zero waiting after physical release, 20% wait more than 0 but no more than 1 h, and 30% wait between 1 and 2 h. The average waiting time is 0.54 h. All 20 ships have zero tardiness, which means all services are completed before the contractual due time. No ship berths earlier than its physical release time or scheduled arrival time, and the schedule is fully operationally feasible. Compared with the arrival-order reference (total waiting 37.43 h, average 1.87 h per ship), the selected schedule reduces average waiting time by 71.1%, significantly improving port operational efficiency. It is worth noting that the average waiting time is higher than the average delay time, which is consistent with the cost coefficient setting: the algorithm prioritizes delay reduction, reflecting the model's tendency to protect supply chain timeliness.

Table 10. Distribution of ship waiting time and tardiness time.

Interval/Statistic	Waiting Count/Value	Waiting (%)	Tardiness Count/Value	Tardiness (%)
0 h	10	50.0	20	100.0
(0, 1] h	4	20.0	0	0.0
(1, 2] h	6	30.0	0	0.0
(2, 3] h	0	0.0	0	0.0
>3 h	0	0.0	0	0.0
Mean h	0.54	—	0.00	—
Early vs. scheduled	0	0.0	—	—

3.3.2. Energy and Cost Reconciliation

To further quantify the peak–valley transfer effect of the optimized schedule, Figure 10 decomposes the aggregate terminal load into shore power hotel load and quay crane load and compares the selected schedule with the arrival-order reference over the 24 h planning horizon. The time-of-use tariff curve is also plotted to visualize the alignment between load distribution and price signals.

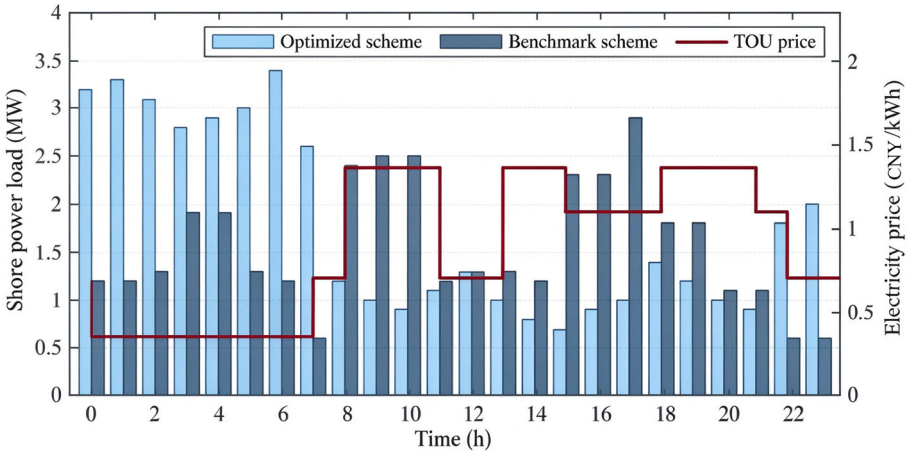


Figure 10. Hourly mean shore power and crane power for the selected schedule and the arrival-order reference. The red line shows the TOU price. Hourly powers integrate to the electricity quantities in Appendix B Table A3; instantaneous peak values are stated separately in the text.

For shore power, the selected schedule has a terminal-wide instantaneous peak of 700 kW, compared with 850 kW in the reference. The load profile shifts noticeably toward the 00:00–07:00 valley period, with sharply reduced draw during sharp-peak hours. For quay crane power, the selected schedule has a peak of 6000 kW, compared with 5250 kW

in the reference; the combined peak of all modeled power is 6700 kW. The higher crane peak in the optimized schedule is a consequence of concentrating handling operations in cheaper hours to reduce total electricity procurement cost, which is an inherent trade-off under the time-of-use pricing mechanism.

In terms of total energy volume, total shore electricity drops from 12,760.83 kWh in the reference to 9792.50 kWh in the selected schedule, while total crane electricity remains constant at 75,150.00 kWh across both schedules. Crane electricity accounts for 88.04% of the total electricity bill in the selected schedule. The invariance of total crane energy follows directly from the inverse scaling relation in Equation (12): total crane work is fixed, so only the tariff time overlap changes across feasible schedules.

The volume-weighted average electricity price falls from 0.8855 CNY/kWh in the reference to 0.7662 CNY/kWh in the selected schedule, a reduction of 13.47%. The share of valley-period electricity rises from 33.92% to 45.18%, confirming the peak-shaving and valley-filling effect of the optimized scheduling. A full event-level energy reconciliation with tier-by-tier breakdowns is provided in Appendix B Table A3.

3.4. Fixed-Schedule Tariff Accounting

This section quantifies electricity bill exposure for the fixed selected schedule under different peak–valley price ratios. The berthing schedule, crane assignments and shore power eligibility remain unchanged; only the tariff level varies. By construction, electricity cost varies linearly with the sharp-peak price for a fixed schedule. This analysis measures cost exposure and does not represent the optimal operational response to a new tariff.

Taking the valley electricity price of 0.3556 CNY/kWh as the benchmark, the sharp peak electricity price is parameterized in five gradients from peak–valley ratio 2:1 to 6:1. We calculate shore power cost, crane cost and total electricity cost separately for the fixed schedule. The results are shown in Figure 11 and Table 11.

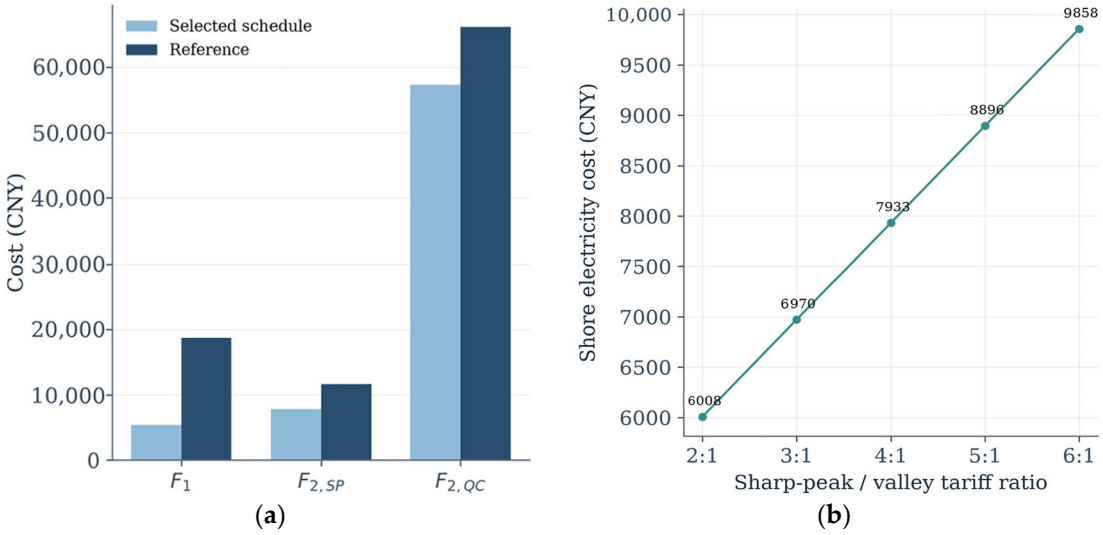


Figure 11. Cost decomposition comparison and fixed-schedule tariff sensitivity analysis. (**a**) Operational cost, shore power cost and quay crane cost for the selected schedule and the arrival-order reference. (**b**) Variation in shore electricity cost with different sharp-peak/valley tariff ratios under the fixed scheduling scheme.

Table 11. Fixed-schedule tariff accounting with separate shore and crane costs.

Sharp/Valley Ratio R	Sharp Rate (CNY/kWh)	Shore Cost (CNY)	Crane Cost (CNY)	Total Cost (CNY)
2:1	0.7112	6007.77	44,247.25	50,255.02
3:1	1.0668	6970.38	51,323.69	58,294.07

4:1	1.4224	7932.99	58,400.13	66,333.12
5:1	1.7780	8895.60	65,476.57	74,372.17
6:1	2.1336	9858.21	72,553.01	82,411.22

As shown in Figure 11a, the selected schedule achieves significant reductions in operational cost, shore power cost and crane cost compared with the arrival-order reference. Figure 11b and Table 11 show the monotonic growth of electricity cost as the peak–valley ratio widens.

Quantitatively, for each unit increase in the sharp/valley ratio R, shore power cost increases by 962.61 CNY and total electricity cost increases by 8039.05 CNY, presenting an exactly linear trend. This linearity is a natural result of the fixed service schedule: the energy volume in each tariff tier is constant, so total cost scales linearly with the sharp-peak price.

Under the baseline TOU scenario used in this paper (sharp/valley ratio ≈ 3.84:1), the total electricity cost of the selected schedule is 65,085.21 CNY, which is consistent with the result in Table 6. This fixed-schedule analysis can be used to quantify the cost exposure of port operations under tariff adjustment, but evaluating the optimal response to a new tariff requires re-optimization under the same computational budget.

3.5. Gross and Net Carbon Effects

Carbon accounting uses the same demand boundary as the scheduling ledger. We relax the idealized full-replacement assumption to account for grid-side emissions, shore power conversion losses, and residual onboard auxiliary generation.

Let D = 9792.50 kWh denote delivered shore electricity at the ship-hotel boundary. The scenario parameters are defined as follows:

- Shore power supply efficiency $\eta = 0.92$;
- Residual onboard generation fraction $\rho = 0.05$;
- Grid emission factor e_{grid} = 0.5703 kg CO_2/kWh;
- Auxiliary engine emission factor e_{aux} = 0.75 kg CO_2/kWh.

All-auxiliary baseline emissions: $E_{\text{baseline}} = D \cdot e_{\text{aux}} = 7344.38\text{kg CO}_2$

Net emissions under the shore power scenario include both residual onboard generation and grid-side supply:

$$E_{\text{shore}} = \rho D e_{\text{aux}} + \frac{(1-\rho)D}{\eta} e_{\text{grid}} = 6133.99\text{kg CO}_2$$

The net CO_2 reduction is 1.21 t (16.48%) relative to the all-auxiliary baseline. At the maximum ship hotel load, the corresponding grid-side demand is 180.71 kW per berth, which remains below the dedicated 400 kW transformer rating.

Limitations: These results are conditional on the stated efficiency and emission factor assumptions, representing a typical scenario rather than verified region/year-specific values. No annual extrapolation is made.

3.6. Fixed Schedule Sensitivity to Bounded Timing Perturbations

To test robustness against navigation uncertainty, we apply bounded perturbations $\varepsilon_i \in [-\delta, \delta]$ to physical release times and both window bounds, with $\delta = 0, 0.25, 0.50\text{h}$. The selected schedule and crane assignments remain fixed throughout the analysis.

Let $w_i = t_i - r_i$ denote the nominal waiting time for ship i. For scenarios where the fixed schedule remains feasible, the attainable bounds of operational cost are derived analytically as

$$F_{1,\min}(\delta) = 500\sum_i \max(w_i - \delta, 0)$$
$$F_{1,\max}(\delta) = 500\sum_i (w_i + \delta)$$

Electricity cost F_2 remains constant at 65,085.21 CNY for all feasible perturbations, as service intervals, crane counts and shore power eligibility are unchanged.

Table 12 summarizes the analytical feasibility margins and attainable objective ranges for the selected schedule. The nominal minimum release margin is 0.00 h and the minimum upper-window margin is 4.30 h. At the two non-zero perturbation levels, the worst-case release margins become negative, meaning feasibility is not guaranteed for every allowed perturbation. Operationally, a negative worst-case release margin means that if a ship's realized release is delayed beyond its nominal slack, its fixed berthing start would fall before the physical release and thus become infeasible; in practice, the port should then postpone that ship's berthing to the realized release time and re-run the greedy repair operator (or a partial re-optimization) to restore feasibility, so the day-ahead schedule should be regarded as a baseline plan requiring online adjustment under large arrival delays rather than one that can be executed rigidly.

Table 12. Fixed-schedule feasibility margins and attainable operational-cost bounds under bounded timing perturbations.

δ (h)	Worst Release Margin (h)	Worst Upper-Window Margin (h)	All Perturbations Feasible	Feasible-Scenario F_1 Range (CNY)	Fixed F_2 (CNY)
0.00	0.00	4.30	Yes	5400.00	65,085.21
0.25	−0.25	4.05	No	4225.00–7900.00	65,085.21
0.50	−0.50	3.80	No	3100.00–10,400.00	65,085.21

These bounds are analytical values conditional on fixed-schedule feasibility, not sample minima/maxima from repeated algorithm runs. The analysis quantifies how arrival-time uncertainty propagates to operational cost under the given scheduling plan.

4. Discussion

This study constructs a bi-objective integrated scheduling model for berths, quay cranes, and shore power in inland river ports under TOU electricity pricing and proposes an improved NSGA-II algorithm embedded with a greedy repair operator and weighted sum scanning strategy for solution. The results verify that the model and algorithm can effectively reduce both operational efficiency cost and electricity purchase cost and achieve significant carbon emission reduction benefits.

Compared with existing studies focusing on seaport scenarios [**Error! Reference source not found.**,**Error! Reference source not found.**,**Error! Reference source not found.**], the innovation of this paper lies in fully considering the unique operational characteristics of inland river ports, including deterministic channel time windows, mandatory shore power compliance constraints, and shore power transformer capacity limits. Case results show that channel time windows and shore power compliance rules significantly shape the scheduling scheme. Under the dedicated transformer topology adopted in this case, the capacity constraint is non-binding for the modeled ship loads; it would become active under shared-transformer topologies or higher per-ship power demand, which cannot be ignored in general inland port planning. In addition, the bi-objective optimization framework adopted in this paper avoids the subjectivity of artificially setting weights, and the obtained Pareto front can provide decision-makers with more flexible decision support.

The improved NSGA-II algorithm with GRO repair operator shows good performance in both solution quality and computational efficiency. For the medium case with

20 ships, the total runtime is 52.6 ± 3.1 s on a single-thread CPU platform, which meets the timeliness requirement of day-ahead port scheduling. The weighted sum scanning strategy effectively improves the diversity and uniformity of Pareto front solutions, providing more alternative schemes for decision-makers with different preferences.

This study also has certain limitations.

1. Electrical topology scope: The reported case uses a dedicated 400 kW transformer per berth, where the capacity constraint is non-binding for the modeled ship loads. The constraint would become active under a shared-transformer topology or higher per-ship hotel loads, which is a natural extension of this model.
2. Static crane assignment: The model assumes fixed crane counts per service with no mid-service reassignment, which aligns with common short-call operations at inland terminals. Dynamic crane allocation and interference effects can be added for terminals with longer vessel calls and flexible crane teams.
3. Tariff analysis nature: The fixed-schedule tariff analysis in Section 3.4 measures cost exposure for a given plan by construction. It does not represent the optimal operational response to a new tariff; full re-optimization under each tariff scenario would be required for policy effectiveness assessment. In addition, systematic re-optimization under different TOU tariff ratios to reveal how price signals reshape scheduling decisions is also a valuable direction for further investigation.
4. Deterministic time windows: The nominal case uses fixed release times and berthing windows. In actual operation, there may be random disturbances in ship navigation. Future research can introduce stochastic optimization or robust optimization methods to deal with arrival time uncertainty.
5. Single terminal scenario: This paper only considers a single terminal scenario and can further expand to multi-terminal collaborative scheduling in port groups. Distributed renewable energy and energy storage systems can also be incorporated into the scheduling framework to improve port energy sustainability.

5. Conclusions

Aiming at the integrated scheduling problem of inland container ports along the Yangtze River Economic Belt under TOU electricity pricing, this paper constructs a bi-objective integer programming model, designs an improved NSGA-II algorithm for solution, and conducts verification through case studies and sensitivity analysis. The model, schedule analysis and repeated-run experiments support the following conclusions:

1. Physical release, scheduled arrival and permissible windows have distinct operational roles. Feasible schedules satisfy $t_i \geq \max(r_i, a_i^L)$ and complete service within the 24 h planning horizon.
2. The selected schedule yields F_1 = 5400.00 CNY and F_2 = 65,085.21 CNY, corresponding to reductions of 71.15% and 16.39% relative to the arrival-order reference. Shore and crane electricity costs decline by 33.19% and 13.43%, respectively. Valley energy share rises from 33.92% to 45.18%, average waiting time falls to 0.54 h, and all ships have zero tardiness. Dedicated 400 kW shore transformers remain non-binding in the case.
3. Under the stated efficiency, residual-generation and emission assumptions, net CO_2 reduction reaches approximately 1.21 t (16.48%) relative to all-auxiliary generation. The result is scenario-conditional and no annual extrapolation is made.
4. With a fixed schedule, electricity cost varies linearly with the peak–valley tariff ratio by construction. This measures bill exposure and does not establish optimal response or policy effectiveness.

5. Across 30 independent runs, the improved NSGA-II reports mean HV 0.810 ± 0.025, IGD+ 0.042 ± 0.006, feasible-run count 30/30, archive size 42 ± 4 and total runtime 52.6 ± 3.1 s. POP = 200 and GEN = 400 provide a balanced quality–runtime configuration. Separately, the bounded fixed-schedule analysis gives attainable F_1 ranges of 4225.00–7900.00 CNY at $\delta = 0.25\text{h}$ and 3100.00–10,400.00 CNY at $\delta = 0.50\text{h}$, conditional on feasibility.

In summary, the proposed method can provide auxiliary decision support for integrated scheduling of inland river ports under TOU electricity pricing scenarios. Future research can further consider the randomness of ship arrival time, multi-terminal collaborative scheduling, and renewable energy access and other extended scenarios.

Author Contributions: Conceptualization, Y.G. and F.S.; methodology, Y.G. and T.C.; software, T.C. and Y.G.; validation, Q.X., F.S. and X.X.; formal analysis, T.C.; investigation, L.B. and Y.G.; resources, F.S. and Q.X.; data curation, Y.G. and T.C.; writing—original draft preparation, Y.G. and T.C.; writing—review and editing, F.S., Q.X. and X.X.; visualization, T.C.; supervision, F.S.; project administration, Q.X.; funding acquisition, F.S. All authors have read and agreed to the published version of the manuscript.

Funding: This work was supported in part by the Open Fund of the State Key Laboratory of Disaster Prevention and Mitigation of Explosion and Impact, Army Engineering University of PLA, under Grant 20260113.

Institutional Review Board Statement: Not applicable.

Informed Consent Statement: Not applicable.

Data Availability Statement: The timing inputs and ship-level schedules are included in Appendix A of the manuscript.

Conflicts of Interest: The authors declare no conflicts of interest.

Abbreviations

The following abbreviations are used in this manuscript:

BAP	Berth Allocation Problem
BAP-QCAP	Integrated Berth Allocation And Quay Crane Assignment Problem
CNY	Chinese Yuan
CO_2	Carbon Dioxide
GEN	Evolutionary Generation Count
GRO	Greedy Repair Operator
HV	Hypervolume
IGD+	Inverted Generational Distance Plus
IMO	International Maritime Organization
MOEA/D	Multi-objective Evolutionary Algorithm Based On Decomposition
NSGA-II	Non-dominated Sorting Genetic Algorithm II
POP	Population Size
QCAP	Quay Crane Assignment Problem
SD	standard deviation
SPEA2	Strength Pareto Evolutionary Algorithm 2
TOU	Time-of-Use

Appendix A. Complete Timing Inputs and Schedule Ledger

Table A1. Complete constructed time inputs and reference crane counts. Window bounds follow the asymmetric −0.5/+6 h rule.

No.	a_i (h)	r_i (h)	a_i^L (h)	a_i^U (h)	d_i (h)	q_i^{ref}
1	0.5	0.7	0.0	6.5	12.5	2
2	3.0	3.2	2.5	9.0	16.0	2
3	6.0	6.2	5.5	12.0	14.0	1
4	10.0	10.2	9.5	16.0	25.0	2
5	0.8	1.0	0.3	6.8	12.8	2
6	4.5	4.7	4.0	10.5	12.5	1
7	12.0	12.2	11.5	18.0	28.0	2
8	0.3	0.5	0.0	6.3	14.3	2
9	3.5	3.7	3.0	9.5	11.5	2
10	6.5	6.7	6.0	12.5	17.5	2
11	11.0	11.2	10.5	17.0	28.0	2
12	1.0	1.2	0.5	7.0	12.0	2
13	5.0	5.2	4.5	11.0	16.0	2
14	9.0	9.2	8.5	15.0	17.0	1
15	0.6	0.8	0.1	6.6	13.6	2
16	4.0	4.2	3.5	10.0	12.0	1
17	8.0	8.2	7.5	14.0	23.0	2
18	0.4	0.6	0.0	6.4	8.4	1
19	4.0	4.2	3.5	10.0	15.0	2
20	8.0	8.2	7.5	14.0	12.6	1

Table A2. (a). Arrival-order reference schedule. Displayed times are rounded to 0.001h; exact service durations follow Equation (12). (b). Selected schedule. Times are in hours; exact durations follow Equation (12).

(a)

No.	Berth	Start h	q_i	T_i (h)	Finish h	s_i	Wait h	Late h
1	3	1.000	3	6.000	7.000	1	0.300	0
2	2	3.500	3	6.667	10.167	1	0.300	0
3	3	9.500	2	2.500	12.000	1	3.300	0
4	5	12.633	3	8.000	20.633	1	2.433	0
5	5	1.300	3	6.000	7.300	1	0.300	0
6	4	7.767	2	2.500	10.267	1	3.067	0
7	6	12.500	3	8.667	21.167	1	0.300	0
8	1	0.800	3	7.333	8.133	1	0.300	0
9	6	6.833	3	3.333	10.167	1	3.133	0
10	2	10.167	3	5.333	15.500	1	3.467	0
11	1	13.467	3	9.333	22.800	1	2.267	0
12	6	1.500	3	5.333	6.833	1	0.300	0
13	1	8.133	3	5.333	13.467	1	2.933	0
14	3	12.000	2	2.500	14.500	1	2.800	0
15	4	1.100	3	6.667	7.767	1	0.300	0
16	3	7.000	2	2.500	9.500	1	2.800	0
17	4	11.867	3	8.000	19.867	1	3.667	0
18	2	0.900	2	2.500	3.400	1	0.300	0
19	5	7.300	3	5.333	12.633	1	3.100	0
20	4	10.267	1	1.600	11.867	0	2.067	0

(b)

No.	Berth	Start h	q_i	T_i (h)	Finish h	s_i	Wait h	Late h
1	3	0.700	4	4.500	5.200	1	0.000	0
2	2	3.200	4	5.000	8.200	1	0.000	0
3	3	7.700	2	2.500	10.200	1	1.500	0

4	1	10.200	4	6.000	16.200	1	0.000	0
5	5	1.000	4	4.500	5.500	1	0.000	0
6	4	5.800	2	2.500	8.300	1	1.100	0
7	6	12.200	4	6.500	18.700	1	0.000	0
8	1	0.500	4	5.500	6.000	1	0.000	0
9	3	5.200	4	2.500	7.700	1	1.500	0
10	2	8.200	4	4.000	12.200	1	1.500	0
11	3	11.200	4	7.000	18.200	1	0.000	0
12	6	1.200	4	4.000	5.200	1	0.000	0
13	1	6.000	4	4.000	10.000	1	0.800	0
14	4	9.900	2	2.500	12.400	1	0.700	0
15	4	0.800	4	5.000	5.800	1	0.000	0
16	6	5.200	2	2.500	7.700	1	1.000	0
17	5	9.500	4	6.000	15.500	1	1.300	0
18	2	0.600	2	2.500	3.100	1	0.000	0
19	5	5.500	4	4.000	9.500	1	1.300	0
20	4	8.300	1	1.600	9.900	0	0.100	0

Appendix B. Supplementary Energy and Experiment Results

Table A3. Energy and operational-cost balance from the same interval and ship ledgers.

Quantity	Unit	Arrival-Order Reference	Selected Schedule
Shore in valley	kWh	3972.03	4028.50
Shore in flat	kWh	1849.04	1842.50
Shore in peak	kWh	2148.37	1214.50
Shore in sharp	kWh	4791.40	2707.00
Crane in valley	kWh	25,850.25	34,350.00
Crane in flat	kWh	11,733.50	13,200.00
Crane in peak	kWh	10,250.25	7700.00
Crane in sharp	kWh	27,316.00	19,900.00
Total shore energy	kWh	12,760.83	9792.50
Total crane energy	kWh	75,150.00	75,150.00
Total energy	kWh	87,910.83	84,942.50
Shore power cost	CNY	11,649.56	7783.56
Quay crane cost	CNY	66,194.19	57,301.65
Total electricity cost	CNY	77,843.75	65,085.21
Valley share	%	33.92	45.18
Waiting cost	CNY	18,717.00	5400.00
Tardiness cost	CNY	0.00	0.00
Total operational cost	CNY	18,717.00	5400.00

Note: All energy values are computed at the idealized scheduling boundary. Event totals are reconstructed from start/completion events and tariff boundaries with half-open intervals. Ledger residuals are evaluated at full numerical precision.

References

1. Channel and Navigation Division of Changjiang Navigation Administration. Green Shore Power Safeguards the Clear Waters and Blue Skies of the Yangtze River. Available online: https://cjhy.mot.gov.cn/xxgk/xxgkzl/hjbh/202408/t20240822_409602.shtml (accessed on 10 June 2026).
2. Economic Information Daily. Built but Hard to Use Vast Shore Power Resources Left Idle Along the Yangtze. *Xinhua News Agency*, 21 January 2021. Available online: https://www.xinhuanet.com/2021-01/21/c_1127006692.htm (accessed on 25 October 2026).

3. Rodrigues, F.; Agra, A. Berth allocation and quay crane assignment/scheduling problem under uncertainty: A survey. *Eur. J. Oper. Res.* **2022**, *303*, 501–524.
4. Wang, Z.; Hu, H.T.; Zhen, L. Berth and quay cranes allocation problem with on-shore power supply assignment in container terminals. *Comput. Ind. Eng.* **2024**, *188*, 109910.
5. Chargui, K.; Zouadi, T.; Sreedharan, V.R. Berth and quay crane allocation and scheduling problem with renewable energy uncertainty: A robust exact decomposition. *Comput. Oper. Res.* **2023**, *156*, 106251.
6. Yang, S.; Shen, H.; Zhong, Z.; Zhang, Y. Collaborative Scheduling for Yangtze Riverport Channels and Berths Using Multi-Objective Optimization. *Appl. Sci.* **2024**, *14*, 6514.
7. Mei, Y.; Han, X. Joint Scheduling of Berths and Quay Cranes Considering Berth Preference and Quay Crane Movement. *Comput. Eng. Appl.* **2022**, *58*, 241–249.
8. Gou, Y.; Liang, C.; Zhang, Y. Research on Joint Scheduling of Berths and Quay Cranes under Time-of-Use Price. *Comput. Eng. Appl.* **2024**, *60*, 338–345.
9. Wang, X.; Dong, Z.; Wang, Y.; Xiao, H. Joint optimization of berth-quay crane-shore power allocation under time-of-use pricing. *J. Transp. Syst. Eng. Inf. Technol.* **2025**, *25*, 314–327. https://doi.org/10.16097/j.cnki.1009-6744.2025.02.029.
10. International Maritime Organization. *Fourth IMO GHG Study 2020*; International Maritime Organization: London, UK, 2020.
11. Ministry of Transport of the People's Republic of China; National Development and Reform Commission; National Energy Administration; State Grid Corporation of China. Notice on Further Promoting Shore Power Use by Ships Berthing in the Yangtze River Economic Belt. 2021. Available online: https://www.gov.cn/zhengce/zhengceku/2021-07/27/content_5627742.htm (accessed on 6 November 2025).
12. Bakar, N.N.A.; Bazmohammadi, N.; Vasquez, J.C.; Guerrero, J.M. Electrification of onshore power systems in maritime transportation towards decarbonization of ports: A review of the cold ironing technology. *Renew. Sustain. Energy Rev.* **2023**, *178*, 113243.
13. Zhang, Y.; Liang, C.; Shi, J.; Lim, G.; Wu, Y. Optimal port microgrid scheduling incorporating onshore power supply and berth allocation under uncertainty. *Appl. Energy* **2022**, *313*, 118856. https://doi.org/10.1016/j.apenergy.2022.118856.
14. Sun, Y.; Guo, Y.; Zhang, Q.; Jia, Y. Berth allocation and energy scheduling for all-electric ships in seaport microgrid: A Stackelberg game approach. *Energy* **2025**, *322*, 135640. https://doi.org/10.1016/j.energy.2025.135640.
15. Ma, K.; Feng, Y.; Yang, J.; Cai, Y.; Yang, B.; Guan, X. Two-stage distributionally robust optimization for port integrated energy system with berth allocation under uncertainties. *Energy* **2025**, *322*, 135588. https://doi.org/10.1016/j.energy.2025.135588.
16. Li, H.; Tai, N.; Yu, M.; Wang, J.; Huang, W.; Huang, Y. Review on energy-logistics coupled optimal dispatching models and methods for port. *Autom. Electr. Power Syst.* **2025**, *49*, 1–21.
17. Deb, K.; Pratap, A.; Agarwal, S.; Meyarivan, T. A fast and elitist multiobjective genetic algorithm: NSGA-II. *IEEE Trans. Evol. Comput.* **2002**, *6*, 182–197.
18. Zitzler, E.; Laumanns, M.; Thiele, L. *SPEA2: Improving the Strength Pareto Evolutionary Algorithm*; TIK Report 103; ETH Zurich: Zurich, Switzerland, 2001. https://doi.org/10.3929/ethz-a-004284029.
19. Zhang, Q.; Li, H. MOEA/D: A multiobjective evolutionary algorithm based on decomposition. *IEEE Trans. Evol. Comput.* **2007**, *11*, 712–731. https://doi.org/10.1109/TEVC.2007.892759.

Disclaimer/Publisher's Note: The statements, opinions and data contained in all publications are solely those of the individual author(s) and contributor(s) and not of MDPI and/or the editor(s). MDPI and/or the editor(s) disclaim responsibility for any injury to people or property resulting from any ideas, methods, instructions or products referred to in the content.